Structure and dynamics of polymer melt confined between two solid surfaces: A molecular dynamics study

3 AUTHORS:

Jalal Sarabadani
Aalto University
26 PUBLICATIONS   **177** CITATIONS

SEE PROFILE

Andrey Milchev
Bulgarian Academy of Sciences
237 PUBLICATIONS   **4,457** CITATIONS

SEE PROFILE

Thomas Vilgis
Max Planck Institute for Polymer Research
389 PUBLICATIONS   **4,253** CITATIONS

SEE PROFILE

Structure and dynamics of polymer melt confined between two solid surfaces: A molecular dynamics study

Jalal Sarabadani, Andrey Milchev, and Thomas A. Vilgis

Articles you may be interested in

Structure and dynamics of confined flexible and unentangled polymer melts in highly adsorbing cylindrical pores
J. Chem. Phys. **141**, 074904 (2014); 10.1063/1.4893055

Internal structure of dendrimers in the melt under shear: A molecular dynamics study
J. Chem. Phys. **121**, 1091 (2004); 10.1063/1.1755659

The effect of bond length on the structure of dense bead–spring polymer melts
J. Chem. Phys. **115**, 2776 (2001); 10.1063/1.1385791

Structure and properties of polymethylene melt surfaces from molecular dynamics simulations
J. Chem. Phys. **115**, 2831 (2001); 10.1063/1.1379536

Molecular dynamics study of polymer melt confined between walls
J. Chem. Phys. **115**, 552 (2001); 10.1063/1.1377015

Structure and dynamics of polymer melt confined between two solid surfaces: A molecular dynamics study

Jalal Sarabadani,[1,2,a)] Andrey Milchev,[1,3] and Thomas A. Vilgis[1]

[1]*Max Planck Institute for Polymer Research, Ackermannweg 10, 55128 Mainz, Germany*
[2]*Department of Applied Physics and COMP Center of Excellence, Aalto University School of Science,*
P.O. Box 11000, FI-00076 Aalto, Espoo, Finland
[3]*Institute of Physical Chemistry, Bulgarian Academy of Sciences, Sofia 1113, Bulgaria*

Using large scale molecular dynamics simulations we investigate the static and dynamic properties of a linear polymer melt confined between two solid surfaces. One of the walls is repulsive and the other is attractive wall. The bottom attractive wall is characterized by different degrees of roughness which is tuned by an array of short perpendicular rigid pillars with variable grafting density. We demonstrate that the conformations of polymers at the interfaces do not depend on substrate-polymer interactions, rather they show similar conformations of a single end-grafted chain under *critical* adsorption condition, consistent with the Silberberg's hypothesis. This observation is found to be in a good agreement with the analysis of the size distributions of trains, loops, and tails of melt chains at the walls known from the theoretical prediction of the end-grafted single chains at critical adsorption. Furthermore, we find that the pressure of the melt P_N decreases as $P_N - P_\infty \propto N^{-1}$ with growing length of the chains N (where P_∞ is the extrapolated pressure for $N \to \infty$). Moreover, the surface tension γ near both walls is found to follow $\gamma_N \propto N^{-2/3}$. Eventually, the lateral dynamics near rough surface drops suddenly when the separation between the neighboring pillars becomes smaller than $2R_g$, where R_g is the bulk radius of gyration. © *2014 AIP Publishing LLC*. [http://dx.doi.org/10.1063/1.4890820]

I. INTRODUCTION

The structural and dynamic properties of linear polymer melts at a solid surface have been the subject of intensive studies by researchers for several decades.[1] This is not only motivated by interest from the fundamental point of view, but also, because of their importance for various applications in surface coatings, lubricants, and composite materials, where these macromolecules control the overall performance of the system.[1,2] More specifically, the presence of surfaces significantly modifies both structural and dynamic properties of macromolecules from that in the bulk. The extent of surface effects and their origin are not well understood and, therefore, Molecular Dynamics (MD) simulations can play a major role to discover them. For example, the effect of the strength of polymer-substrate adsorption, or, instead, the geometric constraints imposed by the confining surface, is still a matter of controversy.[3] One general reason for the lack of full understanding of the problem is the presence of a wide range of time and length scales involved that make the analysis of the experimental data difficult.[4] In this sense, the use of computer-aided modeling for the study of confined polymers has proven to be rewarding. By means of computer simulations, a number of physically relevant quantities that describe the conformation and the relaxation of the polymer can be defined and elucidated in detail. Two main approaches can be recognized in this field. For the case of *atomistic* simulations, where full chemical details are included, some examples are, the studies by Daoulas *et al.*[5] on films of polyethylene on

graphite, Hentschke *et al.*[6] (graphite/alkane), Yelash *et al.*[7] (graphite/polybutadiene), Mansfield and Theodorou,[8] Smith *et al.*[9] (atomistic surface/*n*-alkane), Pandey and Doxastakis[10] (silica/polyethylene). These methods provide a lot of information about polymer behavior at various surfaces as long as the concentrations are not too high. For concentrations approaching melt conditions, however, atomistic simulations are not feasible as a source of reliable statistical data.

Alternatively, one can use *coarse-grained* models whereby some atomistic details are sacrificed in order to be able to treat much larger systems with a proper statistical averaging of the observables. Most frequently, atomistic as well as coarse-grained studies are carried out by means of Monte Carlo (MC),[11–14] and MD methods.[15–23] A rather efficient approach for analysis of structural properties is based on Self-Consistent Field (SCF) models at the level of mean-field approximation.[24–26] As a rule, most of these computer experiments have been focused on the structure and relaxation dynamics of a polymer melt at solid (structureless or atomically smooth) surfaces. It has been demonstrated, however, that differences in the smoothness of the solid boundary may have a major impact, e.g., on fundamental aspects of the glass transition in polymer films (see, for example, Refs. 17–20 and 27–30). A rather important aspect of this problem is the correlation between mechanical, structural, and dynamical properties of polymer nanocomposites.[31,32]

In this work, we investigate the structure and dynamic properties of a polymer melt at solid interfaces, focusing on several aspects that have found so far little or insufficient attention within the context of interfacial melt properties.

a)Electronic mail: jalal.sarabadani@aalto.fi

Following the theoretical predictions of Silberberg,[33] and Skvortsov and Gorbunov,[34] we demonstrate that in a confined melt the chain conformations can be described as random walks with reflecting boundary (the so called Silberberg's hypothesis) and, *irrespective* of the particular interaction between the melt and the solid wall, are nearly identical with the conformations of a *single* chain under *critical adsorption conditions*. Earlier studies of this problem have been using lattice models[3,13,14] whereby, in contrast to continuum models, some typical properties of the melt structure in the vicinity of a solid wall as the well known layering effect cannot be reproduced. Therefore, it remains unclear to what extent the Silberberg's hypothesis holds within the framework of a more realistic (off-lattice) description of the melt/surface region. We examine the probability distributions of the trains, loops, and tails of polymers at the solid surface and find that they closely follow the theoretical predictions by Hoeve[35] and Fleer[24,25] for single chains at criticality.

Another point, examined carefully in the present study, pertains to the pressure, P_N, exerted by the polymer melt on the container walls, and specifically on the impact of chain length N on pressure. We find that $P_N(N) - P_\infty$ diminishes as N^{-1} with chain length, while the surface tension, γ_N, derived from the pressure anisotropy perpendicular and parallel to substrate, varies as $N^{-2/3}$, in agreement with earlier experimental findings.[36–38] Eventually, we examine the impact of surface roughness on polymer dynamics by grafting an array of vertical pillars to the solid wall in contact with the melt, and studying the influence of changing roughness on diffusion dynamics in the vicinity of the boundary plane.[39]

The remainder of the paper is organized as follows: in Sec. II, we introduce the coarse-grained model for the solid/melt system and the parameters of the MD simulation. In Sec. III, we describe our findings regarding the melt structure at the interface, including our test of Silberberg's theory, Sec. III C, and the observed probability distributions of trains, loops, and tails, Sec. III D. Section IV presents our results on pressure and surface tension whereas our investigations of melt structure at rough surface and polymer mobility are shown in Secs. V A and V B respectively. Our conclusions are briefly summarized in Sec. VI.

II. THE MODEL

To study polymer melt near hard surfaces, we use the bead-spring model of the polymer chains.[40] In this model, the bonded interaction between adjacent beads of a polymer is a combination of a finitely extensible nonlinear elastic (FENE) potential,

$$U_{\text{FENE}} = -\frac{k_0}{2} R_0^2 \ln \left[1 - \left(\frac{r}{R_0} \right)^2 \right], \tag{1}$$

where $k_0 = 30$ is the elastic constant, and the maximal extension of the bond between neighboring segments is $R_0 = 1.5$, and the Weeks-Chandler-Anderson (WCA) potential

$$U_{\text{WCA}}(r) = \begin{cases} U_{\text{LJ}}(r) - U_{\text{LJ}}(r_c), & r \le r_c, \\ 0, & r > r_c, \end{cases} \tag{2}$$

where the cut-off radius is $r_c = 2^{1/6}$, and $U_{\text{LJ}}(r)$ is the Lennard-Jones (LJ) potential

$$U_{\text{LJ}}(r) = 4\epsilon \left[\left(\frac{\sigma}{r} \right)^{12} - \left(\frac{\sigma}{r} \right)^6 \right], \tag{3}$$

where ϵ is the depth of the well of the potential, r is the distance between monomers, and σ is the size of each monomer. The quantities are defined in the reduced units, whereby the mass of each monomer is set to $m = 1$, length is expressed in units of the LJ radius $\sigma = 1$, and the energy unit is $\epsilon = 1k_B T$ (k_B denotes here the Boltzmann constant). The temperature, T, is measured in the unit of ϵ/k_B, and the unit of time is $\sigma\sqrt{m/\epsilon}$. For all non-bonded monomer-monomer interactions we have used truncated and shifted LJ potential, Eq. (3), with the cut-off radius of $r_c = 2.5$.

The polymer melt is confined between two surfaces. The surfaces are flat and are modeled as two-dimensional square arrays of beads with lattice constant of $a = \sqrt{2}/2$. The bottom surface is attractive and its beads interact with the monomers via a full LJ potential, shown in Eq. (3). The depth of the potential well is chosen as $\epsilon_{\text{bot}} = 2.0$ and a cut-off radius of $r_{c,\text{bot}} = 2.5$. The interaction between the beads of the top repulsive wall and the monomers is WCA as given by Eq. (2), with $r_{c,\text{top}} = 2^{1/6}$ as the cut-off radius, and $\epsilon_{\text{top}} = 1$.

In order to examine the effect of surface roughness, we have studied two kinds of systems, systems with smooth walls, and also systems with variable roughness, that is, with fixed vertical pillars which are arranged in a regular array on the attractive surface (see Fig. 1). Each pillar is made of 20 fixed beads with radius 1σ and the distance between adjacent beads is 0.5, making the pillars height of 10. Each pillar particle interacts with the monomers through a WCA potential. In some cases, we have also used attractive pillars. Details will be mentioned whenever appropriate.

We have investigated a polymer melt composed of monodisperse linear chains. Three system sizes are chosen with box dimensions of $L_x = 64$, $L_y = 32$, and $L_z = 40$ in Secs. III, IV, and V A, and $L_x = L_y = 16$, and $L_z = 50$ to study systems composed of chains with lengths of $N = 10$ or 20, and $L_x = L_y = 24$, and $L_z = 50$ to study systems composed of chains with length of $N = 30$ in Sec. V B. The periodic boundary conditions are implemented only in the x-y plane. In Secs. III, IV, and V A, the attractive and repulsive surfaces are placed at $z = 0$ and $z = 40$, respectively, and the monomer density is taken as 0.88, whereas in Sec. V B the attractive and repulsive surfaces are placed at $z = 0$ and $z = 50$, respectively, so that a free surface of the melt is formed in the vicinity of the repulsive wall. The chain lengths are varied between 10 $\le N \le 240$, which span from the disentangled to the entangled regime. The ESPResSo++ package has been used to perform the simulations.[41] The equations of motion are integrated using the velocity-Verlet algorithm. The time step is chosen as $dt = 0.005$. The temperature is set to $T = 1$ using a Langevin thermostat with a friction coefficient $\gamma = 0.5$.

In order to create an initial configuration, we first constructed the self-avoiding random-walk polymers, and then we applied the force-capping method[42] so as to eliminate any overlaps between monomers in the system. Then, we ran the integrator with the full interaction to equilibrate the system.
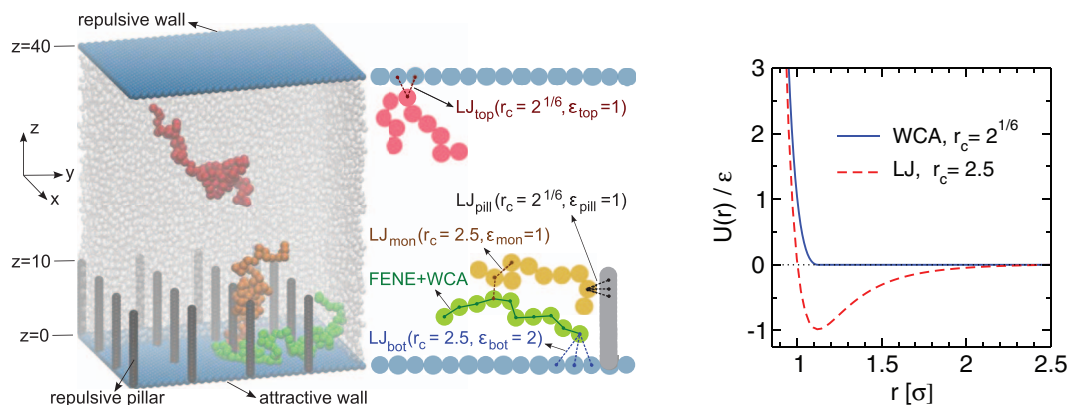
FIG. 1. Left panel: The schematic geometry of the system. The polymer melt is confined between a repulsive- (top), and an attractive wall (bottom). When surface roughness is considered, repulsive pillars with length of 10σ are attached vertically to the attractive wall. A polymer chain in the bulk (red) of the system and two chains (orange and green) near the attractive wall are shown. The box size of the system is $L_x = 64$, $L_y = 32$, and $L_z = 40$. For a better view, we have cut the system and shown only part of it. Middle panel: Different interactions that act in the system. Right panel: Normalized WCA and LJ potentials, $U(r)/\epsilon$, as a function of the distance between two particles, r.

The number of measurements for all systems was 2×10^3, except for the case with chain length of $N = 240$ which was 10^3.

III. CONFORMATION OF POLYMERS IN THE MELT WITHOUT PILLARS

In this section, we consider some properties related to the conformation of polymer chains, such as monomer number density (MND), radius of gyration, and the distribution of loops, trains, and tails in the regions near the attractive and near the repulsive walls. Since the system is anisotropic in the z direction, we study monomer number density and the radius of gyration layer-wise.

A. Monomer density profiles

First, we examine out-of-plane monomer density profile, $\rho_{\mathrm{mon}}(z)$. In Fig. 2, we show ρ_{mon} for three different systems composed of linear polymers with chain lengths of
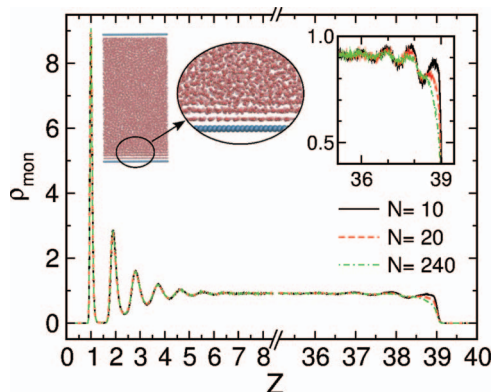

FIG. 2. The monomer density profile, $\rho_{\mathrm{mon}}(z)$, as a function of the distance from the bottom attractive wall, z, for different chain lengths of $N = 10$ (black solid line), 20 (red dashed line), and 240 (green dashed-dotted line). Left inset is devoted to show a real snapshot of the system, where one can easily see the layering effect. In the right inset, the region of $z > 37$ close to the upper repulsive container wall is magnified for better visibility.

$N = 10, 20$, and 240 whereby each unit of length in the z direction has been divided into 100 slabs parallel to the bottom surface. As a rule, data were averaged over 2×10^3 different realizations, and only for the case of $N = 240$ the average was taken over 10^3 measurements. Evidently, one observes a strong layering effect near the attractive surface whereas in the vicinity of the top repulsive surface this effect is weak. Apparently, due to wall attraction the melt monomers are rather densely packed at the bottom wall, therefore all three density profiles coincide. In contrast, the layering in the vicinity of the repulsive surface is only weakly pronounced. This behavior can be explained by monitoring the pressure as a function of chain length, which will be presented in Sec. IV. Since the pressure becomes higher for shorter chain lengths (see Sec. IV), the few layers there are better expressed (cf. the right inset in Fig. 2) for $N = 10$ than for the melts with longer chains.

B. Radius of gyration

Another quantity of interest is the radius of gyration, R_g, which is defined as

$$R_g^2 = \frac{1}{N} \sum_{i=1}^{N} \left(\vec{R}_i - \vec{R}_{\mathrm{cm}} \right)^2, \tag{4}$$

where $\vec{R}_{\mathrm{cm}}$ is the radius-vector of the center of mass of each polymer chain, and the end-to-end distance, R_e. The latter is defined by a slab in the middle of the system with a thickness equal to the radius of gyration. In Fig. 3, we show R_g^2, R_e^2 (end-to-end distance squared), and the z component of the end-to-end distance squared, $R_{e,z}^2$, for the bulk of the linear polymer melt as a function of the chain length N. For a sufficiently long chain, $N \geq 96$, we find a slope of 1, in agreement with the expected exponent of $\nu = 0.5$ for an ideal chain in a melt.[43]

In order to elucidate the effect of walls on the polymer chain conformations, we examine the variation of the parallel, $R_{g\parallel}^2 = \frac{1}{2N} \sum_{i=1}^{N} [(x_i - x_{\mathrm{cm}})^2 + (y_i - y_{\mathrm{cm}})^2]$, and
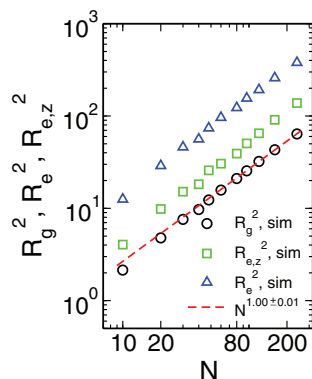
FIG. 3. Squared radius of gyration of polymer chains in the bulk, R_g^2 (open black circles), end-to-end distance, R_e^2 (open blue triangles), and z-component of the latter, $R_{e,z}^2$ (open green squares), against chain length, N, for the system without pillars ($\rho_r = 0$). The line is a power law fit to the data points with $N \geq 96$ with an exponent unity.

perpendicular, $R_{g\perp}^2 = \frac{1}{N} \sum_{i=1}^{N} (z_i - z_{cm})^2$, components of R_g^2. In Fig. 4(a), we show $R_{g\parallel}^2$ and $R_{g\perp}^2$ layer-wise as functions of z, for systems composed of chain lengths of $N = 10, 30$, and 80 segments. It can be seen that near the walls the conformations of the polymers change, i.e., the polymers from the so called pancake conformation, which is reflected by $R_{g\parallel}^2 > R_{g\perp}^2$. Apparently, the changes in the gyration radius components take place within a distance of $R_g(N)$ from the confining planes and are more pronounced for $R_{g\perp}^2$.

In Fig. 4(b), we have displayed the scaling behavior of R_g^2, $R_{g\perp}^2$, and $R_{g\parallel}^2$ for the different regions of the first ($z < R_g$) and the last ($L_z - z < R_g$) layers, and also for the bulk of the system as a function of the chain length, N. The thickness of the first and the last layers, are equivalent to bulk R_g^2 for a particular N. Interestingly, the two components of the gyration radius in the first and in the last layers change in such a way that the *total* radius of gyration in these layers (solid red and open blue circles, respectively) remains equal to that of the bulk region (open black circles) for each chain length.
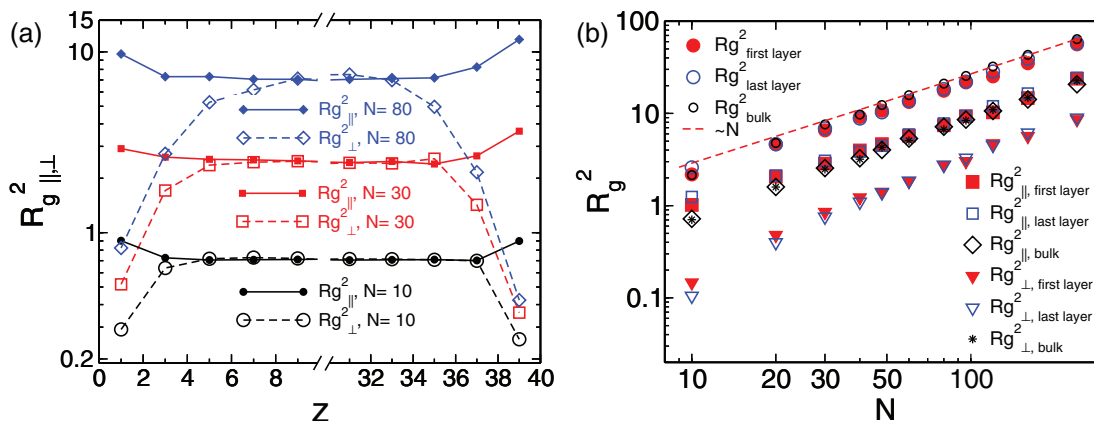
Generally, the variation of the gyration radius components with the distance from the solid wall is not a very sensitive indicator with respect to the melt structure at a solid wall. Nonetheless, it demonstrates that the particular (attractive/repulsive) interactions of the melt with the respective wall make little difference as far as conformational properties of the adjacent macromolecules are concerned.

C. Test of Silberberg's hypothesis

Using our simulation data, we test the "random walk next to reflective boundary" predictions of Silberberg[33] who interpreted the observed mean contraction of macromolecules at the vicinity of a solid-melt interface in terms of a set of principles for "conformation transfer," which involves "segmental swapping" between unconstrained chains with regard to the confining hard wall. The polymer chains are labeled by their "starting monomer" (that is, by the chain end closest to the solid surface). Silberberg's procedure of reflection of configurations reproduces the dominant feature of a solid-(incompressible) melt interface, namely, the nearly constant density on a scale coarser than the statistical segment size. Bitsanis and ten Brinke,[13] however, pointed out that the consistency with the modeling of chains as Gaussian coils requires that the "reflective" boundary condition be applied to *statistical*, rather than actual, segments even though the statistical segment inside the interface cannot be identical with those in the bulk. Therefore, in the present subsection we test to what extent the presence of interface (as, e.g., the observed layering immediately at the walls) affects Silberberg's predictions.

One possible test to check for the validity of Silberberg's "random walk next to a reflective boundary" statistics in reproducing actual chain conformations at solid-melt interfaces, is presented in Fig. 5 where we compare simulation data for the "chain start" probability $P_{start}(z)$ with the corresponding analytical result.[33] Evidently, P_{start} is equal to $1/2$ in the bulk (i.e., each chain end may be the closer one with 50% probability), and approaches unity immediately at the wall where the

FIG. 4. (a) Parallel ($R_{g\parallel}^2$) and perpendicular ($R_{g\perp}^2$) components of squared radius of gyration, as function of z for three different chain lengths of $N = 10, 30, 80$, respectively. (b) R_g^2 for the bulk (open black circles), for the first layer (filled red circles), for the last layer (open blue circles), $R_{g\parallel}^2$ for the bulk (open black diamonds), first layer (filled red squares), last layer (open blue squares), and $R_{g\perp}^2$ for the bulk (black stars), first layer (filled red triangles), last layer (open blue triangles), as function of chain length, N. The first layer is at the attractive wall and its thickness is equal to the radius of gyration in the bulk of the system, while the last layer is at the repulsive wall and has the same thickness as the first layer.
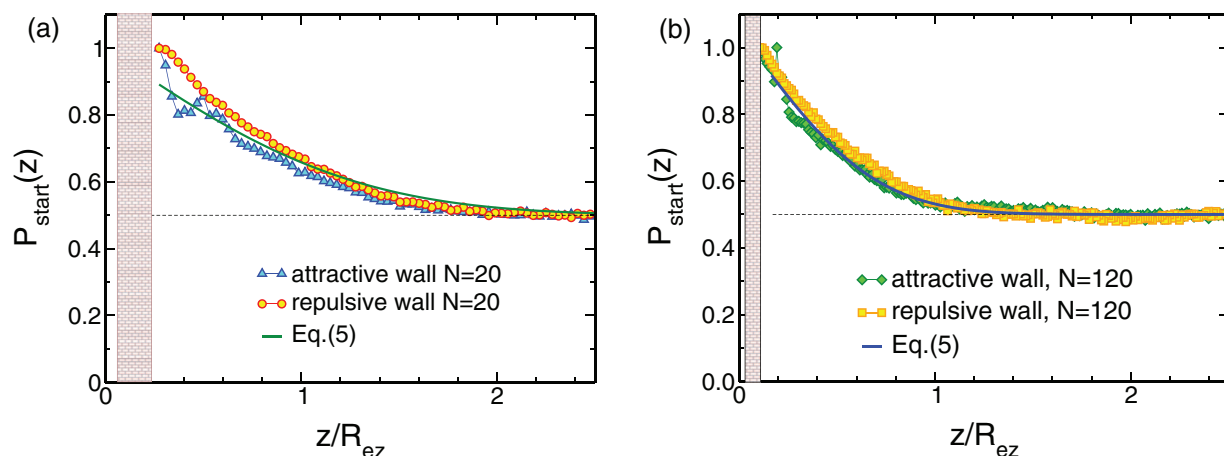
FIG. 5. (a) Chain start profiles, $P_{start}(z)$, i.e., the probability that a chain end found at a particular distance z from the surface, for chain length $N = 20$ with respect to the attractive wall (blue triangles) and with respect to the repulsive wall (red circles). A chain start is defined as the chain end closest to the surface. The green solid line is the analytical prediction. (b) The same as (a) but for chain length $N = 120$.

chance to find the second chain end equally close vanishes. For $P_{start}(z)$, one has[33]

$$P_{start}(z) = 1 - \frac{1}{2}\mathrm{Erf}\left(\frac{z}{\sqrt{2}R_z}\right). \tag{5}$$

It can be seen that the simulation data agree reasonably well with the prediction, in Eq. (5), for *both* walls apart from some oscillations at the attractive surface due to the layering effect. The small fluctuations due to the layering (packing) effects, however, are beyond the scope of Silberberg's approach. Indeed, one may see in Fig. 5 that, regardless of chain length, the data nearly collapse irrespective of whether the solid surface attracts or repels the polymers.

Another hallmark of the "reflection of configurations" is the accumulation of chains centers of mass at a distance $z_0 = \sqrt{\frac{2}{\pi}}R_{gz}$ from the walls,[13] where R_{gz} denotes the z-component of the bulk radius of gyration, see Fig. 6. In Figs. 6(a) and 6(b), such an increase is also well pronounced, followed

by a sharp depletion due to excluded volume effects of the monomers, roughly one monomer diameter away from the wall.

Actually, the chain center of mass profile, $\rho_{CM}(z)$, following from a continuous random walk profile next to a reflective wall, which is

$$\rho_{CM}(z) = \frac{1}{\mathrm{Erf}\left(\frac{z}{\sqrt{2}N}\right)}, \tag{6}$$

should diverge when $z \to z_0$,[33] as indicated in Figs. 6(a) and 6(b). In real and simulated melts, however, this divergence does not occur owing to the breakdown of the random flight description on the monomer scale. Instead, $\rho_{CM}(z)$ increases at z_0, in agreement with the "reflective boundary" condition, and then sharply declines at distances of $z \approx \sigma$ (a bead diameter) due to excluded-volume effects on the scale of individual repeat units. This is shown in Figs. 6(a) and 6(b) to happen at both surfaces roughly at the position of the predicted divergence (the profiles, Eq. (6), are indicated there by full solid lines). Apparently, the peaks that replace these divergences, sharpen with growing chain length N whereby the peaks are pushed away from the surface and become broader for short chains. This effect has been interpreted[13] as resulting from the competition between packing requirements and long chain conformational needs which is resolved differently depending on the length of the polymers. For much longer chains, however, this effect vanishes altogether.

Eventually, we examine the concentration profiles perpendicular to the walls for chains whose starting ends reside immediately or very closely to one of the walls so that such chains may be considered like being incidentally "grafted" to the solid surface. For the latter, a continuum model for a *single* end-attached chain under *critical conditions* provides analytical solutions[44] for the overall distribution of chain segments, $\phi_0(z)$, as well as for that of chain ends, $\phi_e(z)$

$$\phi_e(z) = \frac{1}{\sqrt{\pi}R_g}\exp(-\zeta^2), \tag{7a}$$

$$\phi_0(z) = \frac{2}{\sqrt{\pi}R_g}[\exp(-\zeta^2) - \sqrt{\pi}\zeta\,\mathrm{Erfc}(\zeta)], \tag{7b}$$

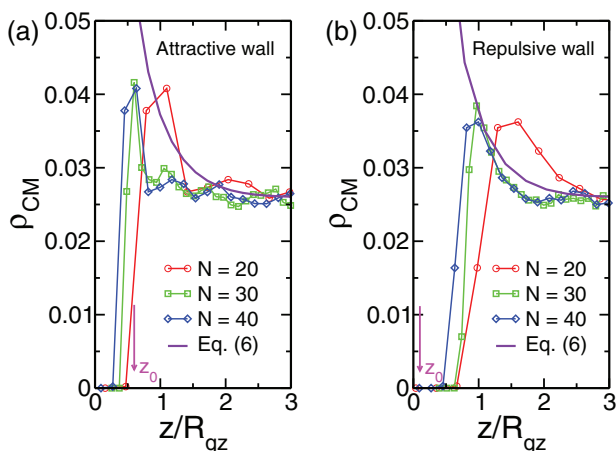

FIG. 6. (a) Normalized profiles of the center of mass density distribution $\rho_{CM}(z)$, for different values of the chain length, $N = 20, 30$, and 40, near the bottom attractive wall as a function of z/R_{gz}, where R_{gz} is the z-component of the bulk radius of gyration, while the theoretical results for random walks is indicated by a solid line. (b) The same as (a), but near the top repulsive wall. In (a) and also (b) $z_0 = \sqrt{\frac{2}{\pi}}R_{gz}$.
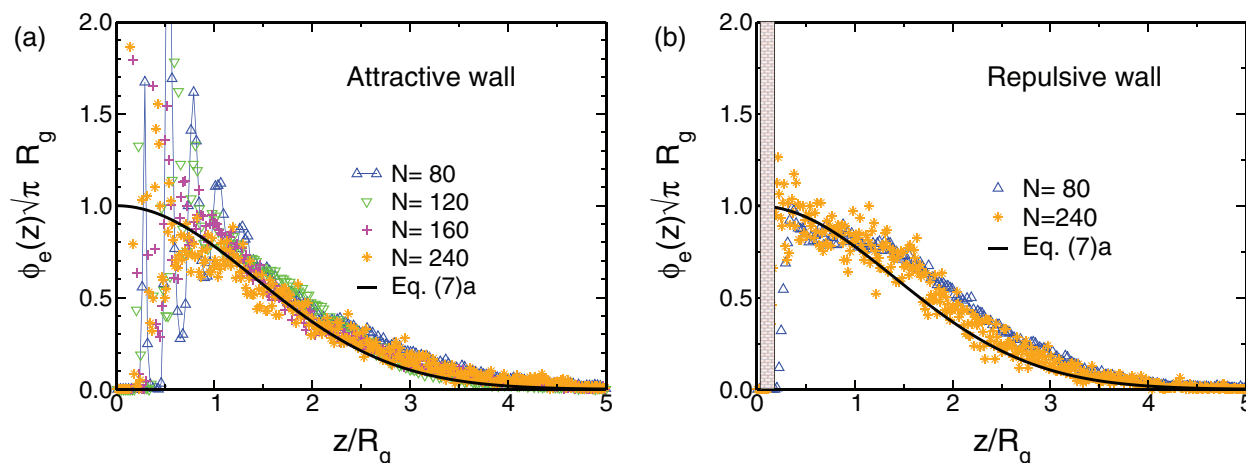
FIG. 7. Density distribution profiles of end-monomer $\phi_e(z)$ (symbols) vs distance from the solid attractive (a) and repulsive (b) walls z in a polymer melt with chain lengths $N = 80, 240$. Chains are selected and analyzed whenever their ends incidentally touch the walls so that such chains may be considered as temporally "grafted." Solid lines denote the analytic result for ideal Gaussian chains, Eq. (7).

where $\zeta = z/(2R_g)$ denotes the dimensionless reduced distance to the wall, and Erfc(x) is the complementary error-function. It is well known that at the critical adsorption point (CAP), the weak attraction exerted by a flat surface on a single chain compensates the entropy loss of the polymer in the surface region, i.e., segment enrichment goes over to depletion so that the probability to find a chain at some distance z from the wall does not depend on z. One could argue that at the CAP the surface is, therefore, invisible and the "reflective boundary conditions" apply.[33] One may readily verify from Figs. 7 and 8 that all the chains of the melt that incidentally happen to touch with an end-monomer either the attractive or the repulsive walls of the container reveal all- and end-segment density distribution along z that are in very good agreement with the corresponding distributions, Eqs. (7), of a single chain at criticality. This important conclusion from Figs. 7 and 8 has also been drawn by Skvortsov et al.[3] who applied the SCFT approach (i.e., the Mean-Field Approximation) to a melt on a cubic lattice.

In fact, both a mushroom conformation of a single chain tethered to a repulsive surface, or a pancake conformation of

adsorbed single chain on attractive surface transform at high concentrations (in the melt) into the same half-Gaussian conformations of a random walk reflected by that surface, regardless of whether the melt adheres or not to the surface plane.[3,33] The oscillations, due to packing and layering at the walls, Figs. 7 and 8, of course, are not accounted for by the analytic theory.[33] One may easily verify from Figs. 7 and 8 that these oscillations stretch only over $\approx 5\sigma$ and do not depend on the length of the macromolecules N. Apart from these oscillations, however, one may argue that chain conformations in the melt can be indeed described as random walks reflected at the solid surface.

D. Distribution of loops, trains, and tails

In this subsection, we consider the distributions of trains, tails, and loops of the chains as main building units of the chain architecture near the attractive and repulsive walls. We start by defining the loops, trains, and tails in our representation. All successive monomers of a chain which are located closer than $z = 1.4$ to the wall are considered (somewhat
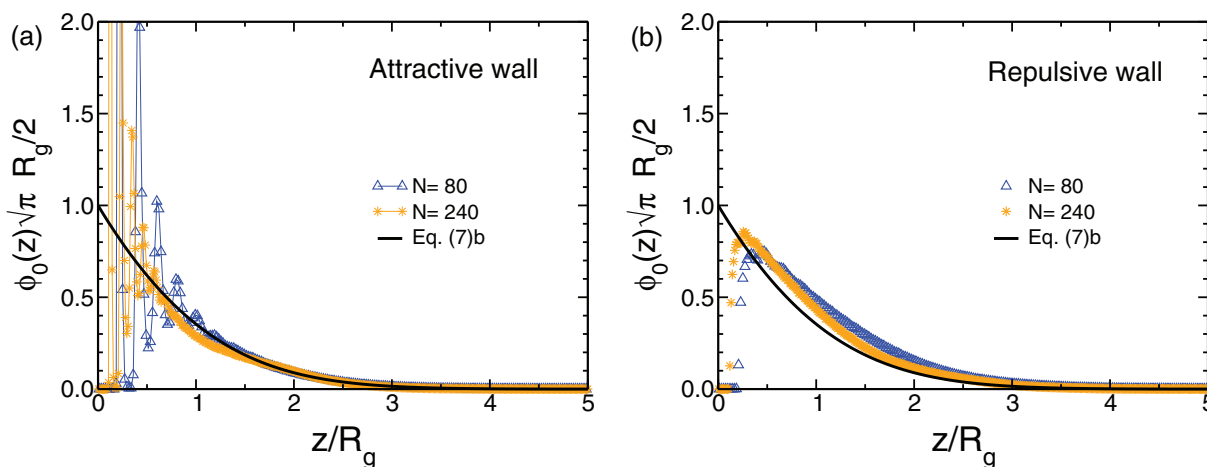

FIG. 8. Monomer density profiles $\rho_{mon}(z)$ (symbols) vs distance z from an attractive (a) and repulsive walls (b) for two different chain lengths $N = 80, 240$ in a melt. Lines denote the analytic expressions for a Gaussian chain, $\phi_0(z)$, Eqs. (7).

arbitrary) as belonging to a train while all monomers along the chain backbone that are located between two successive trains define a loop. Monomers of each end of the chain that are located in a region with $z > 1.4$ then define a tail. Since there are detailed predictions about the size distribution of trains, loops, and tails for *single* chain under critical conditions,[24,35,44,45] we compare our simulation results with the theoretical predictions.

In Fig. 9(a), we have plotted the distribution of the loops near the repulsive (top panel) and near the attractive (bottom panel) walls as function of loop length, s, for different values of chain length $N = 80, 120, 160,$ and 240. The black dashed lines denote the expected power law function $s^{-3/2}$. Evidently, apart from some deviations for the shortest loops (note that the logarithmic scale exaggerates the importance of the shortest scale), $s \leq 4$, and the inevitably deteriorating statistics of the longest loops measured, one observes a rather good agreement in the intermediate region of s where reliable statistics is available. In Fig. 9(b), the normalized distribution of chain tails near repulsive (top panel) and attractive (bottom panel) walls have been shown as function of tail length, s, for the same chain lengths as in (a). Again it can be verified from Fig. 9(b) that the distribution of tails (which covers a broad range of tail sizes), is perfectly described by the power law function $s^{-0.5}$. Merely in the normalized distribution of trains near the two walls, Fig. 9(c), one finds some deviation (an initial power law relationship at small sizes) from the predicted exponential dependence, $\exp(-s/\langle s \rangle)$, where $\langle s \rangle$ is the mean value of trains lengths. The (negative) slope of the exponential distribution is also a little bit higher than the inverse mean value $\langle s \rangle$. We believe that this is caused by some uncertainty (arbitrariness) in the definition of the trains itself, which makes the distinction between very short trains and flat loops in continuous models a matter of convention. As it can be seen from

the respective insets, longer trains (on average) can be found near the attractive wall in comparison with the repulsive one.

Summarizing, the analysis of the size distributions of all three building units of chains that are in contact with the solid walls of our simulation box suggest again that the polymer chains in the melt behave exactly as single chains at zero concentration at the CAP. It should be noted too that these findings support similar results pertaining to the probability distributions of trains, loops, and tails, derived recently on a lattice.[3]

IV. PRESSURE

Now, we want to study how does the pressure profile depend on chain length. We calculate the pressure tensor as a sum of the kinetic, P_K, and virial, P_U, parts.[16] As the system under consideration is in mechanical equilibrium, the statistical averages of all pressure tensor off-diagonal elements are equal to zero. Furthermore, due to symmetry, the lateral components of the pressure tensor, P_{xx} and P_{yy}, are also equal.

We define the pressure tensor as $P(z) = \mathbf{e}_z \mathbf{e}_z P_\mathrm{N}(z) + (\mathbf{e}_x \mathbf{e}_x + \mathbf{e}_y \mathbf{e}_y) P_\mathrm{T}(z)$, where $\mathbf{e}_x$, $\mathbf{e}_y$, and $\mathbf{e}_z$ are unit vectors in x, y, and z directions, respectively. We compute $P_\mathrm{N}(z)$ and $P_\mathrm{T}(z)$ layer-wise by means of Irving and Kirkwood's (IK) method.[46] According to Ref. 46, the contribution of pairwise forces between particles to the virial is taken into account, if the connecting line of the centers of mass of these particles intersects the infinitesimal surface of $d\vec{A}(z)$. The pressure tensor P is defined as $d\vec{F} = -d\vec{A} P$ where $d\vec{F}$ is an infinitesimal force. Starting from the definition of the virial part of pressure, P_U,[47] and using IK method, one can get the following expressions for the average values of the normal, $P_{zz} = P_\mathrm{N}(z)$, and tangential, $P_\mathrm{T}(z)$, components of the pressure tensor:

$$P_\mathrm{N} = \rho(z) k_\mathrm{B} T - \frac{1}{2A} \left\langle \sum_{i \neq j} \frac{|z_{ij}|}{r_{ij}} U'(r_{ij}) \Theta\left(\frac{z - z_i}{z_{ij}}\right) \Theta\left(\frac{z_j - z}{z_{ij}}\right) \right\rangle,$$

$$P_\mathrm{T} = \rho(z) k_\mathrm{B} T - \frac{1}{4A} \left\langle \sum_{i \neq j} \frac{x_{ij}^2 + y_{ij}^2}{r_{ij}} \frac{U'(r_{ij})}{|z_{ij}|} \Theta\left(\frac{z - z_i}{z_{ij}}\right) \Theta\left(\frac{z_j - z}{z_{ij}}\right) \right\rangle,$$

$$(8)$$

where A is the surface area of the system parallel to the $x - y$ plane, $\rho(z)$ is monomer density, averaged over lateral coordinates x and y, $\langle \bullet \rangle$ denotes statistical average, and the summation runs over all pairs of particles. In Eqs. (8), r_{ij} is the distance between the ith and jth particles (that can be either monomers, or mixture of walls particles and monomers), which is defined as $\mathbf{r}_{ij} = \mathbf{r}_i - \mathbf{r}_j$, i.e., $r_{ij} = |\mathbf{r}_{ij}|$ and x_{ij}, y_{ij}, and z_{ij} are three components of $\mathbf{r}_{ij}$. The force between particles i and j is the derivative $-U'(r_{ij})$ of the potential U, and $\Theta(x)$ is the Heaviside step function. In Eqs. (8), the first terms are the kinetic contributions to the pressure. We have combined the following

identity:

$$|z_{ij}| \Theta\left(\frac{z - z_i}{z_{ij}}\right) \Theta\left(\frac{z_j - z}{z_{ij}}\right) = -z_{ij}[\Theta(z_i - z)\Theta(z - z_j) - \Theta(z_j - z)\Theta(z - z_i)],$$

$$(9)$$

with Eqs. (8) to calculate the normal and tangential components of the pressure tensor, i.e., P_N and P_T, respectively.

In Fig. 10, we plot the out of plane pressure profile for a system which contains chains with length of $N = 10$. Here, we also show various contributions to P_N. The total sum of these contributions is apparently constant in the z-direction,
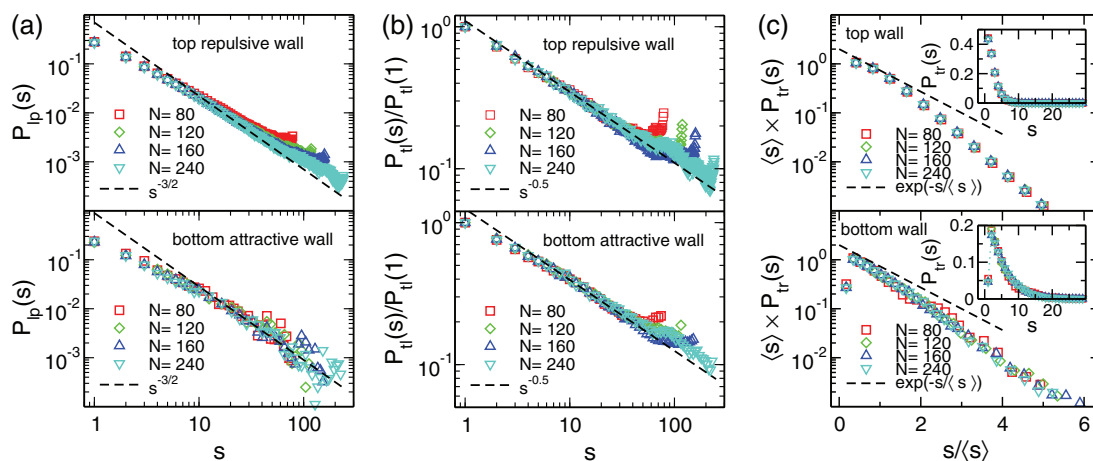
FIG. 9. (a) Distribution of loops near repulsive wall (top panel), and near attractive wall (bottom panel), as function of loop length, s, for different values of chain length $N = 80$ (red squares), 120 (green diamonds), 160 (blue upward triangles), and 240 (turquoise downward triangles). The black dashed lines denote the function $s^{-3/2}$ in both panels. (b) Normalized distribution of tails near repulsive (top panel) and near attractive (bottom panel) walls as function of tail length, s, for the same values of chain length as of (a). The black dashed lines indicate the function $s^{-0.5}$ in both panels. (c) Normalized distribution of trains near repulsive (top panel) and near attractive (bottom panel) walls as function of normalized train length, $s/\langle s \rangle$, where $\langle s \rangle$ is the mean value of train length, for the same values of N as in (a) and (b). The insets show the distribution of trains as a function of train length, s, in normal coordinates. Dashed lines denote the functional relationship $\exp(-s/\langle s \rangle)$.
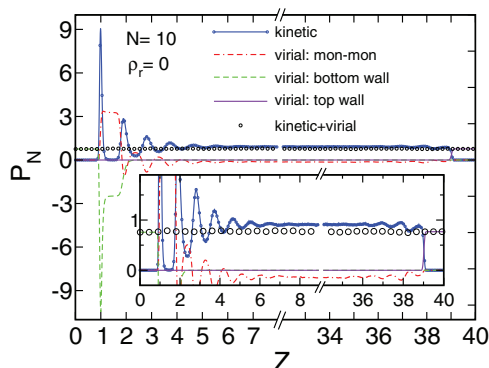

FIG. 10. Different contributions of the zz component of the pressure tensor, $P_N(z)$, due to the kinetic part (blue circles line), the virial part of monomer-monomer interactions (red dashed-dashed-dotted line), the virial contribution of the bottom attractive wall particle-monomer interactions (green dashed line), and the virial contribution of the top repulsive wall particle-monomer interactions (violet solid line), for a system composed of chains with length of $N = 10$. Apparently, the sum of the kinetic and the total virial contributions (black circles) is constant across the container, as expected in equilibrium. The inset shows a part of the main graph with higher resolution.

corresponding to the state of mechanical equilibrium. Evidently, the effect of both the bottom and top surfaces vanishes when the distance from them exceeds 8σ and 4σ, respectively, but these contributions have to be taken into account in order to achieve uniform pressure in z-direction throughout the box. The kinetic part of P_N near the bottom attractive wall strongly oscillates reflecting the pronounced layering effect caused by the competition between the attractive wall-monomer and the repulsive excluded volume interactions. Near the top repulsive wall this layering effect is weaker as the monomers are not attracted by the wall.

The change of pressures P_N as a function of chain length, N, in shown in Fig. 11 for several grafting densities of pillars, ρ_r. The pressure was thereby measured in the region $z > 20$ for systems with $\rho_r \neq 0$, since the Irving-Kirkwood method is valid only for those systems that have lateral translational symmetry,[46] while for systems with $\rho_r = 0$ the pressure was measured across the whole systems. Expectantly, cf. inset in Fig. 11, one observes a systematic increase in P_N with
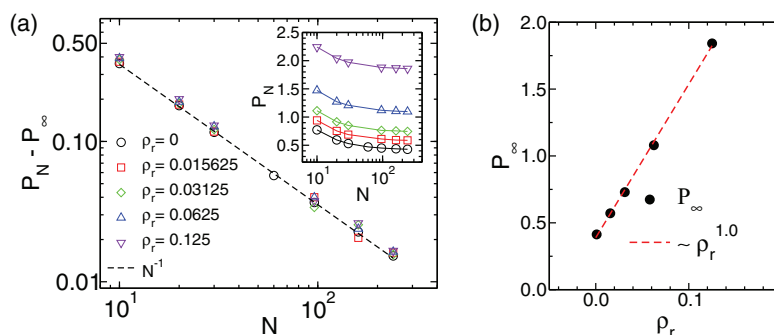

FIG. 11. (a) Inset: P_N has been plotted as a function of chain length, N, for a smooth walls and various values of the density of pillars, $\rho_r = 0$ (black circle line), 0.015625 (red square line), 0.03125 (green diamond line), 0.0625 (blue upward triangles line), and 0.125 (violet downward triangles line). In the main panel, $P_N - P_\infty$ has been shown as a function of chain length, N, for the same values of the density of pillars as in the inset. (b) P_∞ (filled black circles) has been plotted as a function of grafting density of pillars, ρ_r. The red dashed line is a fitting curve with the exponent of 1.

growing pillar density ρ_r, owing to the induced decrease of total accessible volume in the container, cf. Fig. 11(b).

Generally, the pressure P_N is observed to steadily decline with growing chain length N, so one may extrapolate it to the limit $N \to \infty$ and measure P_∞ for each value of ρ_r. Interestingly, the difference $P_N - P_\infty$ then collapses onto a single master curve, $P_N - P_\infty \propto 1/N$, irrespective of pillar density. This finding is fully in agreement with the theoretical predictions for systems with pair interactions.[48] Indeed, by subtracting P_∞ from the zz-element of the total pressure tensor, P_N, the kinetic part of the pressure will remain, which is proportional to the number of objects (polymer chains) in the system. On the other hand, since the concentration of chain ends changes as $2/N$ with chain length N, and (the more loosely bound) chain ends tend to explore a larger volume than inner monomers in the macromolecules, the decline of pressure $P_N - P_\infty$ with growing N is ascribed to chain-end effects.[49–51] This decrease of pressure with growing length of the polymers in the melt nicely agrees with the observed weaker layering at the upper wall, see the right inset in Fig. 2, as the monomers are less tightly packed.

To gain a feeling about the magnitude of the pressure exerted by melt on the walls, here we estimate their order of magnitudes. The typical MD simulation units of the length and time for the bead-spring model are $\sigma = 0.5$ nm and $t_0 = 3$ ps and for the pressure is $P_0 = 40$ MPa.[20] For the shortest chain length $N = 10$, and without any pillar, $\rho_r = 0$, the value of the pressure in MD units which is $P_N \sim 0.75$ [M.D. units] can be written in real units as $P_N \sim 30$ MPa. This is equivalence to the force exerted by melt on the walls which is $f = P_N \times A = P_N \times L_x L_y \sigma^2 \sim 0.015$ μN. For the case of $N = 10$ and highest grafting density of pillars $\rho_r = 0.125$ the pressure has its highest value (in the present work) which is $P_N \sim 2.24$ [M.D. units] ~ 89.6 MPa, and the respective forces on the walls are $f \sim 0.046$ μN. And the least value for the pressure (in the present work) is observed in the system with $N = 240$ and $\rho_r = 0$ as $P_N \sim 0.43$ [M.D. units] ~ 17.2 MPa and the related exerted force on the walls is $f \sim 0.009$ μN.

Another important quantity, also considered in the present section, is the surface tension of the polymer melt near the bottom attractive and near the top repulsive walls (for a system without pillars). The surface tension, can be calculated by integrating the asymmetry of the pressure tensor, $P_N - P_T$, over z[16,52,53]

$$\gamma_{\text{bot}} = \int_{z=0}^{z=D_1} [P_N(z) - P_T(z)] dz,$$
$$\gamma_{\text{top}} = \int_{z=D_2}^{z=40} [P_N(z) - P_T(z)] dz, \tag{10}$$

where D_1 and D_2 denote appropriate distances from the two walls where the normal and tangential components of the pressure tensor are statistically the same, i.e., $P_N(z = D_1) - P_T(z = D_1) = 0$.

In Fig. 12, we plot the surface tension γ at both interfaces of the system. Subtracting the extrapolated value of γ_∞ for infinitely long chains, $N \to \infty$, one observes a power-law relationship, $\gamma(N) - \gamma_\infty \propto N^{-n}$ with an exponent n
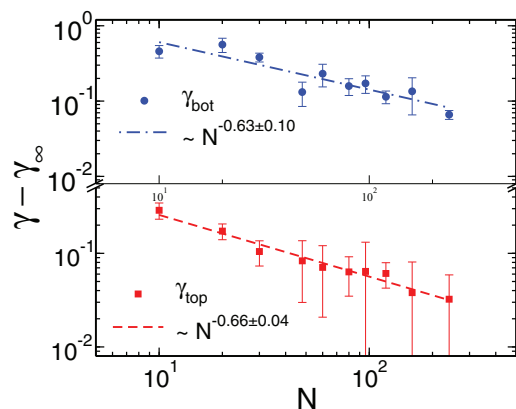

FIG. 12. Surface tension of the melt at the bottom attractive wall, γ_{bot}, and at the top repulsive wall, γ_{top}, as function of the chain length, N. In both cases, the extrapolated value γ_∞ for $N \to \infty$ has been subtracted. The measured exponent n of $\gamma - \gamma_\infty \propto N^{-n}$ agrees closely with the experimentally measured value of $n = 2/3$.[36–38]

$\approx 0.66 \pm 0.04$ which agrees very well with the experimental measurements of linear perfluorinated alkane melts,[36–38] and with the predictions of the Cahn-Hilliard theory[54,55] for planar interfaces. Here, one should note that a stronger dependence, $\gamma \propto N^{-1}$, has also been observed in experiments on poly(tetrafluoroethylene) (PTFE), especially for higher molecular weight of the polymers.[37] As demonstrated by Sauer and Dee,[37] the Cahn-Hilliard theory reproduces all of these experimentally observed changes of γ with the molecular weight so both the $N^{-2/3}$ to N^{-1} dependence of γ are well described, provided bulk pressure-volume-temperature properties are fitted with the equation of state theory of Flory, Orwoll, and Vrij.[56] Sauer and Dee[37] assumed thereby, that the surface has the same composition as the bulk, so this theory should fail in the cases where significant orientation occurs at the free surface. More recently, R. B. Thompson et al.,[57] using SCFT, reproduced the behavior of $\gamma(N)$ with molecular weight for both lower and higher molecular weight polymers and interpreted the change as being due to the decreasing interface width with growing N.

It should be emphasized, however, that these reports have been challenged.[38,49,58] In particular, Aubouy et al.,[58] predicted a relationship $\gamma(N) = \gamma_\infty + const. \frac{\ln(N/N^*)}{\sqrt{N}}$ (where N^* plays the role of a characteristic molecular weight of the polymer under consideration), in very good agreement with experimental measurements. In particular, for $N < N^*$ their result is equivalent to $\gamma = \gamma_\infty - const \cdot N^{-n}$ with an apparent exponent n that is both larger than 1/2 and an increasing function of N. Their theory has been based on the analysis of the size distribution of loops in the conformations of adsorbed chains, and on some additional conjectures (inter alia, assumed attraction of chain ends to the hard wall, impenetrability of the adsorbed layer by the free chains of the melt) whose validity and mutual consistency remains to some extent disputable. Unfortunately, however, the data for our longest chains, $N = 240$, derived with the error bars from this MD study, exclude a higher accuracy check of n in this respect.
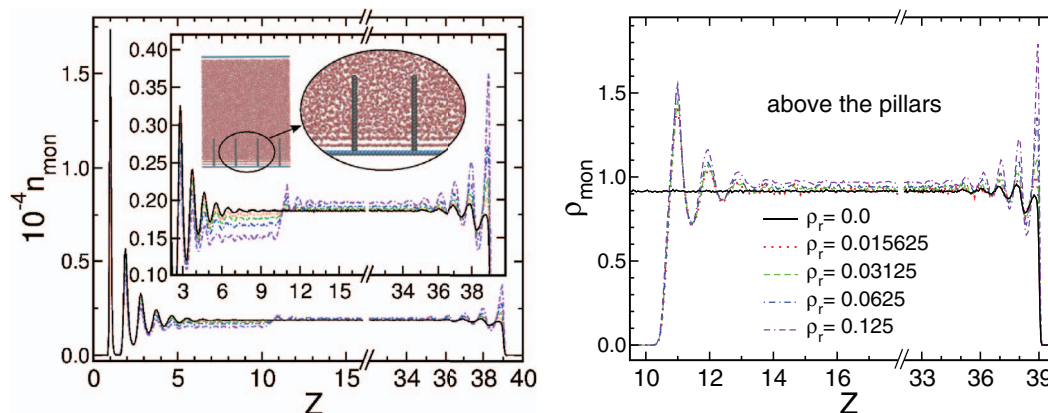
FIG. 13. (Left) The number of monomers, n_{mon}, vs distance z from the bottom wall, for a system with $N = 10$, and different densities of the pillars, ρ_r, grafted at $z = 0$. Here, $\rho_r = 0$ (black solid line), 0.015625 (red dotted line), 0.03125 (green dashed line), 0.0625 (blue dashed-dotted line), and 0.125 (violet dashed-dashed-dotted line). The inset displays a local magnification of the system. (Right) Monomer density profiles, $\rho_{mon}(z)$, around the top of each pillar, for chains of length $N = 10$ and various grafting densities of pillars, ρ_r, as indicated.

V. EFFECTS OF SURFACE ROUGHNESS

A. Melt structure at rough surface

The effects of surface roughness, i.e., when the bottom attractive wall is covered with pillars, are presented in Fig. 13. Here, we keep the chain length constant, $N = 10$, and vary the grafting density of the pillars, ρ_r, between zero (i.e., smooth substrate) and $\rho_r = 0.125$. It can be seen that with growing pillar density, an additional layering occurs between $10 < z < 16$. As the distance between the attractive and repulsive walls is thereby kept constant, this effect becomes more pronounced when the grafting density of the pillars is increased, which reduces the total accessible volume. This is consistent with the increased pressure. As a matter of fact, for the largest grafting density of pillars, $\rho_r = 0.125$, the plane immediately at the top of the pillars behaves like a second pseudo-surface that supports the melt with only few or no polymer chains beneath as a Wenzel-Cassie-like wetting transition.

Note that in Fig. 13 (left panel) we actually show the *monomer number*, n_{mon}, as a function of z (i.e., in a narrow slab Δz), and *not* the monomer density when pillars are present. The reason is that, strictly speaking, in order to find ρ_{mon}, one should divide the number of monomers in each

layer by the volume accessible to the monomers in the layer. Finding accurate values for the effective accessible areas for *each* layer, however, is very difficult since it requires precise knowledge of the excluded volume, occupied by the pillars themselves, which is hardly possible. Notwithstanding, we show how the presence of pillars affects ρ_{mon}, in Figs. 13 (right panel) and 14 where we have plotted it in the regions above and around the pillars, respectively.

Thus, Fig. 13 (right panel) shows ρ_{mon} in the region above each pillar in z direction. In this figure, we have again plotted $\rho_{mon}(z)$ for one chain length of $N = 10$ and different grafting densities of the pillars, $0 \le \rho_r \le 0.125$. The accessible volume *above* each pillar is calculated as a cylinder with a diameter of 1σ. It can readily be seen that by increasing the number of pillars in the system the layering effect above pillars becomes more pronounced.

Layering can also be expected radially from the pillars. In Fig. 14, we have plotted MND around each pillar for a system with fixed chain length of $N = 10$ and $\rho_r = 0.015625$, as a function of z and x, or y (the lateral distance from each pillar in x or y directions respectively, denoted by red arrows in Fig. 14(a)), and r (the lateral distance from each pillar in the diagonal direction, denoted by a blue arrow in Fig. 14(b)). As
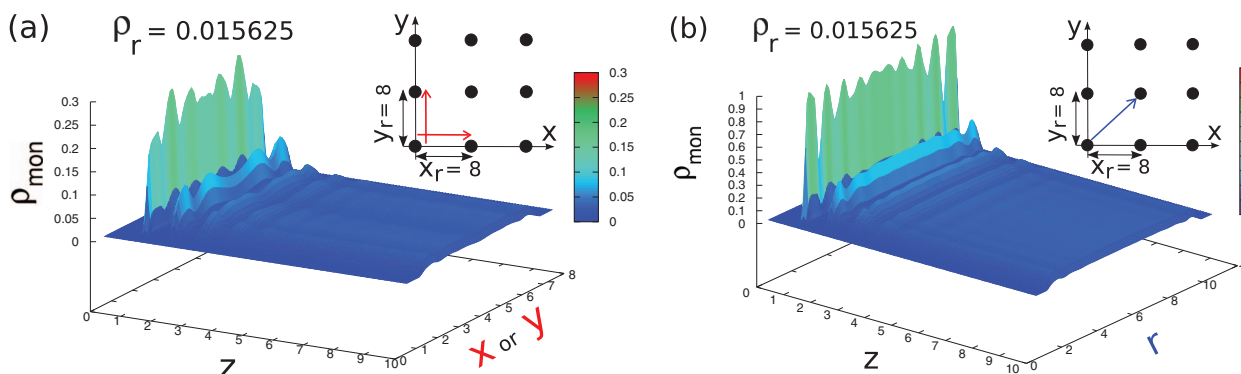

FIG. 14. (a) MND, ρ_{mon}, around pillars as a function of the lateral distance from each pillar in x or y direction, respectively (red arrows in the inset), for a system with fixed chain length of $N = 10$ and pillars grafting density of $\rho_r = 0.015625$. (b) The same as (a) but as a function of the distance from each pillar, r, in the diagonal direction (blue arrow in the inset).
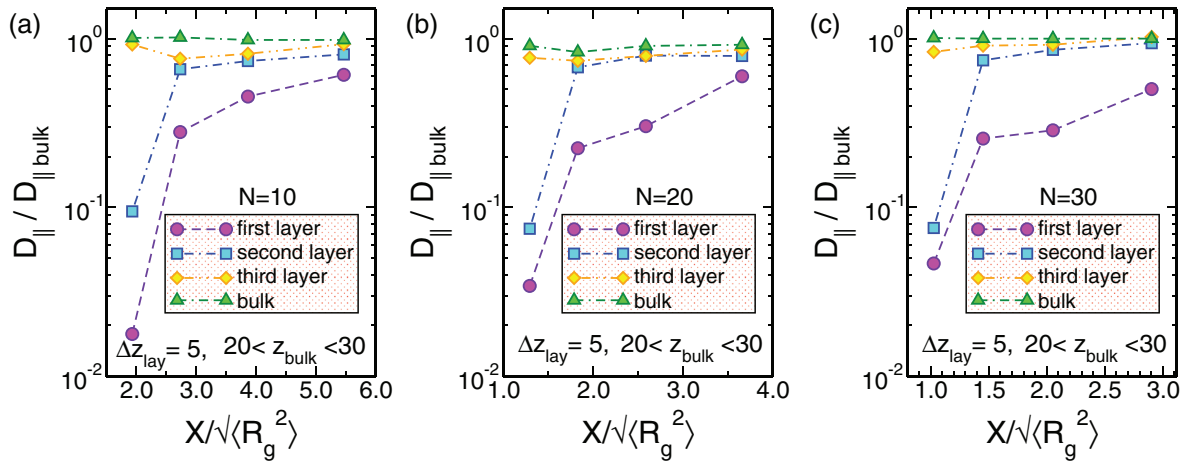
FIG. 15. (a) Normalized diffusion coefficient of the system for the dynamics parallel to the attractive surface as function of the distance X between pillars, normalized by the mean value of the radius of gyration in the bulk of the system, $\sqrt{\langle R_g^2 \rangle}$. Data from different regions of the first layer (black circle-dashed line), second layer (black square-dashed line), third layer (black diamond-dashed line) as well as bulk of the system (black triangles-dashed line) are shown. Here, $N = 10$. (b) The same as (a), but for a system composed of linear chains with length $N = 20$. (c) The same as (a) and (b), but for a system composed of linear chains with length $N = 30$.

far as the pillars are placed on a square lattice array, the system does not have local lateral translational symmetry around each pillar at fixed distance of z, so one must calculate $\rho_{\text{mon}}(z)$ around the pillars locally. The latter, therefore, reveals differences for fixed z in x-, or y-direction with respect to the diagonal direction, depicted in Figs. 14(a) and 14(b). Evidently, the rather complex picture of the layering around the pillars results both from the interaction of monomers with the attractive wall and also with the repulsive pillars.

B. Mobility of monomers in the melt

Finally, we examine the polymer dynamics near solid interface. In order to study the influence of the different levels of the roughness on the melt dynamics at interfaces, we consider systems with different grafting densities of pillars as explained in Sec. II. Here, however, the interactions between pillar particles and the monomers are described by attractive Lennard-Jones forces with a cut-off radius of 2.5 and a potential well depth of $\epsilon_{\text{pill}} = 2$. In this way, the pillars are energetically indistinguishable from the attractive wall for the melt and thus it is only the topological effect that influences chain dynamics.

Since the normal component of the pressure, P_N, for a fixed volume depends on the grafting density of the pillars, ρ_r, (see Fig. 11), in order to compare the dynamics of the systems in the vicinity of the attractive surface to that in the bulk, we moved the upper repulsive wall up to a new height, $z = 50$, creating thus a free surface of the melt under that upper wall, keeping thus the melt always at zero normal pressure.

As before, the melt dynamics stays thus anisotropic due to the presence of two interfaces and has to be analyzed layer-wise. To this end, we divide the system into layers (slabs) and examine the polymer mobility in four qualitatively different slabs. The slabs are chosen parallel to the surfaces and have thickness of 5σ except for the bulk layer which has the thickness of 10σ. To calculate the mean-squared-

displacement (MSD) parallel to the surfaces, we introduce the z-dependent MSD of monomers parallel to the surfaces in each slab, similar to previous investigations[17,27] as

$$g_0^{||}(z, t) = \left\langle \frac{1}{n_t} \sum_i \prod_{t'=0}^{t} \delta(z - z_i(t')) \left| r_i^{||}(t) - r_i^{||}(0) \right|^2 \right\rangle, \quad (11)$$

where we have taken into account only those n_t monomers ($n_t = \sum_i \prod_{t'=0}^{t} \delta(z - z_i(t'))$) that remain in the first ($0 < z < 5$), second ($5 < z < 10$), and third ($10 < z < 15$) layers, and also in the bulk at all times $t' \leq t$. In Eq. (11), we have assumed that the distance between the center of mass of each slab from the bottom attractive surface is z.

In Fig. 15, we show the relative (dimensionless) diffusion coefficient of the system, normalized by the values in the bulk, for the dynamics parallel to the attractive rough surface. The quantity $D_{||}/D_{||\text{bulk}}$ is studied as function of the distance between nearest neighboring pillars, X, in units of the mean value of the radius of gyration in the bulk, $\sqrt{\langle R_g^2 \rangle}$. In the first layer near the attractive surface, the mobility of the monomers is significantly reduced by nearly two orders of magnitude. The decrease in $D_{||}/D_{||\text{bulk}}$ becomes dramatic whenever $X/\sqrt{\langle R_g^2 \rangle} \leq 2$. Below this threshold, the distances separating neighboring pillars create bottlenecks for the polymer coils. As the melt here consists of comparatively short chains with no mutual entanglements, the strong decline in parallel diffusion suggests that polymer coils at $X/\sqrt{\langle R_g^2 \rangle} \leq 2$ are trapped between neighboring pillars. The latter form cavities (i.e., effective traps) so that escape from such a trap may be accomplished only by means of a different type of dynamics, namely, by reptational motion. Of course, in the present case the traps themselves are not purely entropic since the pillars attract the polymer chains as strongly as the solid surface.

Similar observation is also found for the second layer (slab II). It can be seen that the reduction in diffusion coefficient is not as pronounced as in slab I. In the third layer,

which corresponds to the slab immediately *above* the pillars (slab III), however, no surface effects are observed and the polymers behave as if in a bulk phase.

On the ground of these findings one may conclude, therefore, that surface roughness dramatically slows down chain dynamics whenever the size of the polymers in the melt goes below the characteristic scale of surface roughness.

VI. CONCLUSION

We have studied the properties of a polymer melt at a solid surface by means of MD simulations of a coarse-grained bead-spring model of homopolymers. The system structure and dynamic properties in the vicinity of attractive/repulsive walls have been studied for polymers of different length N as well as for different degree of roughness of the confining solid surface.

Our investigations demonstrate that the conformational properties of the chains in a melt in contact with impenetrable solid surface resemble closely those of a single polymer chain at a plane under critical adsorption conditions, in agreement with the Silberberg hypothesis. The observed contraction of polymer coils, chain-end enrichment, and monomer density profiles perpendicular to the surface agree well with the analytical expressions describing ideal (Gaussian) chains as random walks with reflective boundary conditions. This conclusion is corroborated by the observed probability distributions of trains, tails, and loops of macromolecules in the vicinity of the walls, regardless of the particular interaction between wall and surface atoms. Differences on the scale of few segment diameters from the wall, however, are clearly seen within the present continuum model and are attributed to packing/layering effects resulting from the interplay between surface confinement and excluded-volume interactions between segments.

The present study of the melt pressure in a slit has revealed that with the growing of the chain length, N, the pressure, $P_N - P_\infty$, decreases as $1/N$. Using the anisotropy of the pressure tensor perpendicular and parallel to the solid boundary one can calculate the surface tension, γ_N, that at the solid substrates declines as $\gamma_N - \gamma_\infty \propto N^{-2/3}$ with increasing the chain length, which is in good agreement with experimental observations.

Eventually, we have found a dramatic drop in the mobility of polymers close to the confining surfaces when the typical scale of surface roughness becomes comparable or drops below the mean coil size in the bulk of the melt. We interpret the observed drop in polymer mobility as a manifestation of the crossover from Rouse- to reptation dynamics that polymers undergo in this case.

ACKNOWLEDGMENTS

[1]G. J. Fleer, M. A. Cohen-Stuart, J. M. H. M. Scheutens, and T. Cosgrove, *Polymers at Interfaces* (Chapman-Hall, London, 1993).
[2]S. Wu, *Polymer Interface and Adhesion* (Marcel Dekker, New York, 1982).
[3]A. M. Skvortsov, F. A. M. Leermakers, and G. J. Fleer, J. Chem. Phys. **139**, 054907 (2013).
[4]F. Varnik and K. Binder, Int. J. Mater. Res. **100**, 1494 (2009).
[5]K. Ch. Daoulas, V. A. Harmandaris, and V. G. Mavrantzas, Macromolecules **38**, 5780 (2005); V. A. Harmandaris, K. Ch. Daoulas, and V. G. Mavrantzas, *ibid.* **38**, 5796 (2005).
[6]R. Hentschke, B. L. Schurmann, and J. P. Rabe, J. Chem. Phys. **96**, 6213 (1992).
[7]L. Yelash, P. Virnau, K. Binder, and W. Paul, Phys. Rev. E **82**, 050801(R) (2010).
[8]K. F. Mansfield and D. N. Theodorou, Macromolecules **22**, 3143 (1989); **23**, 4430 (1990); **24**, 4295 (1991); **24**, 6283 (1991).
[9]G. D. Smith, D. Y. Yoon, and R. L. Jaffe, Macromolecules **25**, 7011 (1992).
[10]Y. N. Pandey and M. Doxastakis, J. Chem. Phys. **136**, 094901 (2012).
[11]R. Pandey, A. Milchev, and K. Binder, Macromolecules **30**, 1194 (1997).
[12]J. Baschnagel, K. Binder, and A. Milchev, in *Polymer Surfaces, Interfaces, and Thin Films*, edited by A. Karim and S. Kumar (World Scientific Publ. Co., Singapore, 2000). p. 1.
[13]I. A. Bitsanis and G. ten Brinke, J. Chem. Phys. **99**, 3100 (1993).
[14]A. Cavallo, M. Müller, J. P. Wittmer, A. Johner, and K. Binder, J. Phys. Condens. Matter **17**, S1697 (2005).
[15]I. Bitsanis and G. Hadziioannou, J. Chem. Phys. **92**, 3827 (1990).
[16]F. Varnik, J. Baschnagel, and K. Binder, J. Chem. Phys. **113**, 4444 (2000).
[17]S. Peter, H. Meyer, and J. Baschnagel, J. Polym. Sci. B **44**, 2951 (2006).
[18]T. G. Desai, P. Keblinski, and S. K. Kumar, J. Chem. Phys. **128**, 044903 (2008).
[19]G. D. Smith, D. Bedrov, and O. Borodin, Phys. Rev. Lett. **90**, 226103 (2003).
[20]D. Mukherji and M. H. Müser, Macromolecules **40**, 1754 (2007).
[21]R. G. Winkler, T. Matsuda, and D. Y. Yoon, J. Chem. Phys. **98**, 729 (1993).
[22]T. Matsuda, G. D. Smith, R. G. Winkler, and D. Y. Yoon, Macromolecules **28**, 165 (1995).
[23]A. De Virgiliis, A. Milchev, V. G. Rostiashvili, and T. A. Vilgis, Eur. Phys. J. E **35**, 97 (2012).
[24]J. M. H. M. Scheutjens and G. J. Fleer, J. Phys. Chem. **84**, 178 (1980).
[25]G. J. Fleer, J. van Male, and A. Johner, Macromolecules **32**, 825 (1999).
[26]G. J. Fleer, J. van Male, and A. Johner, Macromolecules **32**, 845 (1999).
[27]J. Baschnagel and F. Varnik, J. Phys.: Condens. Matter **17**, R851 (2005).
[28]P. Scheidler, W. Kob, and K. Binder, Europhys. Lett. **59**, 701 (2002); J. Phys. Chem. B **108**, 6673 (2004).
[29]P. M. Adriani and A. K. Chakraborty, J. Chem. Phys. **98**, 4263 (1993).
[30]S. Peter, S. Napolitano, H. Meyer, M. Wübbenhorst, and J. Baschnagel, Macromolecules **41**, 7729 (2008).
[31]A. Kutvonen, G. Rossi, and T. Ala-Nissila, Phys. Rev. E **85**, 041803 (2012).
[32]S. T. Knauert, J. F. Douglass, and F. W. Starr, Macromolecules **43**, 3438 (2010).
[33]A. Silberberg, J. Colloid Interface Sci. **90**, 86 (1982); **125**, 14 (1988).
[34]A. M. Skvortsov and A. A. Gorbunov, Polymer Sci. U.S.S.R. **28**(9), 2159 (1986).
[35]C. A. J. Hoeve, E. A. Di Marzio, and P. Peyser, J. Chem. Phys. **42**, 2558 (1965).
[36]D. G. Legrand and G. L. Gaines, J. Colloid Interface Sci. **31**, 162 (1969).
[37]B. B. Sauer and G. T. Dee, Macromolecules **27**, 6112 (1994).
[38]S. Wu, J. Macromol. Sci. - Rev. Macromol. Chem. **C10**, 1 (1974).
[39]M. Kapnistos, M. Lang, D. Vlassopoulos, W. Pyckhout-Hintzen, D. Richter, D. Cho, T. Chang, and M. Rubinstein, Nat. Mater. **7**, 997 (2008).
[40]G. S. Grest and K. Kremer, Phys. Rev. A **33**, 3628 (1986).
[41]J. D. Halverson, T. Brandes, O. Lenz, A. Arnold, S. Bevc, V. Starchenko, K. Kremer, T. Stuehn, and D. Reith, Comput. Phys. Commun. **184**, 1129 (2013).
[42]R. Auhl, R. Everaers, G. S. Grest, K. Kremer, and S. J. Plimpton, J. Chem. Phys. **119**, 12718 (2003).

[43]M. Doi and S. F. Edwards, *The Theory of Polymer Dynamics* (Oxford University Press, 1986).

[44]E. Eisenriegler, K. Kremer, and K. Binder, J. Chem. Phys. **77**, 6296 (1982).

[45]L. I. Klushin, A. A. Polotsky, H.-P. Hsu, D. A. Markelov, K. Binder, and A. M. Skvortsov, Phys. Rev. E **87**, 022604 (2013).

[46]J. H. Irving and J. G. Kirkwood, J. Chem. Phys. **18**, 817 (1950).

[47]J.-P. Hansen and I. R. McDonald, *Theory of Simple Liquids* (Academic, London, 1990).

[48]R. K. Pathria, *Statistical Mechanics* (Butterworth Heinemann, 2001).

[49]A. N. Semenov, J. Phys. II (France) **6**, 1759 (1996).

[50]J. Bonet Avalos, J.-F. Joanny, A. Johner, and A. N. Semenov, Europhys. Lett. **35**, 97 (1996).

[51]A. A. Shvets and A. N. Semenov, J. Chem. Phys. **139**, 054905 (2013).

[52]J. S. Rowlinson and B. Widom, *Molecular Theory of Capillarity* (Clarendon, Oxford, 1982).

[53]A. Milchev and K. Binder, J. Chem. Phys. **114**, 8610 (2001).

[54]J. W. Cahn and J. E. Hilliard, J. Chem. Phys. **28**, 258 (1958).

[55]C. I. Poser and I. C. Sanchez, J. Colloid Interface Sci. **69**, 539 (1979).

[56]P. J. Flory, R. A. Orwoll, and A. Vrij, J. Am. Chem. Soc. **86**, 3507 (1964).

[57]R. B. Thompson, J. R. MacDonald, and P. Chen, Phys. Rev. E **78**, 030801(R) (2008).

[58]M. Aubouy, M. Manghi, and E. Raphaël, Phys. Rev. Lett. **84**, 4858 (2000).